ACADEMIC PRESS

Available online at www.sciencedirect.com
SCIENCE DIRECT®

Journal of Catalysis 214 (2003) 292–307

JOURNAL OF CATALYSIS

www.elsevier.com/locate/jcat

The effect of CO_2 and H_2O on the kinetics of NO reduction by CH_4 over a La_2O_3/γ-Al_2O_3 catalyst

Todd J. Toops, Arden B. Walters, and M. Albert Vannice *

Department of Chemical Engineering, The Pennsylvania State University, University Park, PA 16802-4400, USA

Received 13 August 2002; revised 22 October 2002; accepted 4 November 2002

Abstract

NO reduction by CH_4 over a 40% La_2O_3/γ-Al_2O_3 catalyst in the absence and presence of O_2 in the feed was studied. The addition of either CO_2 or H_2O to the feed produced a reversible inhibitory effect on the rate similar to that observed with unsupported La_2O_3; however, the extent of rate inhibition was considerably smaller than on unsupported La_2O_3. At 973 K, either CO_2 (9%) or H_2O (2%) in the feed decreased activity by about 35% in the absence of O_2 and by only 20% with excess O_2 in the feed. In the absence of O_2, a reaction mechanism previously proposed for La_2O_3 was altered to include competitive CO_2 and H_2O adsorption and to give the following rate expression for N_2 formation:

$$r_{N_2} = \frac{k' P_{NO} P_{CH_4}}{(1 + K_{NO} P_{NO} + K_{CH_4} P_{CH_4} + K_{CO_2} P_{CO_2} + K_{H_2O} P_{H_2O})^2}.$$

This equation fit the data well, had apparent activation energies of 14–25 kcal/mol, and gave thermodynamically consistent enthalpies and entropies of adsorption. Stable rates at 973 K with O_2 and either CO_2 or H_2O in the feed were between 0.94 and 0.99 μmol N_2/s/g catalyst. In the presence of excess O_2, after CO_2 and H_2O adsorption were again included, a rate equation proposed earlier for La_2O_3 again provided a good fit to the data with H_2O in the feed as well as thermodynamically consistent parameters determined under integral reaction operation. However, with both CO_2 and excess O_2 in the feed, this rate expression could not provide thermodynamically meaningful parameters from the fitting constants even though it fit the data well. This was attributed to a major contribution from the alumina to the overall rate, because CO_2 had no significant effect on NO reduction on alumina, but it inhibited this reaction on La_2O_3. A reaction model was proposed for γ-Al_2O_3 that gave the rate expression for total CH_4 disappearance due to both combustion and NO reduction over γ-Al_2O_3

$$(r_{CH_4})_T = \frac{k'_{com} P_{CH_4} P_{O_2}^{0.5} + k'_{NO} P_{NO} P_{CH_4} P_{O_2}^{0.5}}{(1 + K'_{NO_2} P_{NO} P_{O_2}^{0.5} + K_{CH_4} P_{CH_4} + K_{O_2}^{0.5} P_{O_2}^{0.5} + K_{CO_2} P_{CO_2} + K_{H_2O} P_{H_2O})^2},$$

which gave a satisfactory fit to the data along with thermodynamically consistent parameters. The second term in this equation, which represents the rate of N_2 formation, was then combined with the rate equation for N_2 formation on pure La_2O_3 in the presence of O_2 to describe overall catalyst performance, and the data were fit well, assuming that La_2O_3 composed 6.8% of the total surface area, a value close to that of 6.1% obtained from XRD line-broadening calculations.

Keywords: NO reduction; CH_4; SCR; Kinetics; La_2O_3/Al_2O_3

1. Introduction

La_2O_3 has one of the most active surfaces above 773 K for the selective catalytic reduction (SCR) of NO by CH_4 [1–4]; however, its surface area is typically very low, which results in low rates and limits any industrial applications. Dispersing La_2O_3 on Al_2O_3 enhances its surface area and increases reaction rates (g^{-1}), and a 40 wt% La_2O_3/γ-Al_2O_3 catalyst was the most active at higher temperatures, with rates comparable to those on zeolite catalysts [5,6]. Flue gas components such as CO_2 and H_2O can adversely affect SCR of NO on these systems, including La_2O_3 [7], and steam is known to facilitate sintering in γ-Al_2O_3 [8–11]; therefore, it is of interest to determine the impact of CO_2 and

* Corresponding author.
E-mail address: mavche@engr.psu.edu (M.A. Vannice).

0021-9517/03/$ – see front matter
doi:10.1016/S0021-9517(02)00092-1

H_2O on La_2O_3/Al_2O_3 catalysts. This study has examined NO reduction by CH_4 over 40% La_2O_3/γ-Al_2O_3 as well as over the γ-Al_2O_3 support between 773 and 973 K in the presence and absence of O_2. The standard concentrations of the flue components were the same as in earlier studies of La_2O_3 and Sr-promoted La_2O_3 [7,12–14], i.e., 9% CO_2 and 2% H_2O. SO_2 was not investigated here because it poisoned La_2O_3 [7]. Reaction orders were determined along with specific activities and activation energies, and reaction mechanisms accounting for the effects of CO_2 and H_2O in the absence or presence of O_2, as well as the concurrent direct combustion of CH_4, were proposed. The equilibrium adsorption constants for CH_4, NO, O_2, CO_2, and H_2O, which were obtained from the optimized rate expressions, were further analyzed to verify their thermodynamic consistency. The catalysts were characterized before and after the kinetic experiments using X-ray diffraction (XRD), BET surface area measurements, and NO chemisorption.

2. Experimental

The supported catalyst was prepared as described elsewhere with La acetate (Molycorp, 99%, 14.64% in H_2O) as the La source and γ-Al_2O_3 (Englehard, 150 m^2/g), using an incipient wetness technique [13,14]. The catalyst was dried at 400 K in air, calcined at 1023 K for 4 h under 50 cm^3 (STP) O_2/min, cooled, and stored in a desiccator. Surface areas from N_2 physisorption, NO chemisorption at 300 K, and XRD patterns of each sample were determined before and after reaction as described elsewhere [7]; however, a brief summary is as follows. XRD spectra were obtained ex situ over a 2θ range of 10°–80° at a scan speed of 5.0°/min and a step size of 0.02° using a Philips MPD X-ray diffractometer with Cu-K_α radiation (40 kV and 20 mA). The N_2 BET isotherms were determined volumetrically in an adsorption system with a base pressure in the sample cell $\leqslant 1 \times 10^{-5}$ Torr using a Mensor DPG II Model 15000 pressure transducer with 0.01% full scale accuracy. Fresh samples (ca. 0.15 g) were treated for 1 h at 400 K in flowing He, evacuated to the base pressure, cooled to 300 K, and then submerged in a liquid N_2 bath. Chemisorption of NO was measured in the same volumetric system after a standard pretreatment of heating from room temperature to 973 K at 11 K/min under 20 cm^3 (STP)/min of 10% O_2 in He, holding for 1 h, evacuating for 30 min, and cooling to 300 K. The sample was evacuated for 1 h at 300 K after the initial isotherm, and a second isotherm was measured to establish reversible adsorption. NO chemisorption on the catalyst after various times on stream was measured after flushing with He at 973 K, cooling to 300 K and measuring NO isotherms and BET surface areas, in that order [7].

The kinetic studies were performed in a reactor system similar to that described previously [15], except that a P-E Sigma 3 gas chromatograph (GC) with a 2.4-m Chromosorb 102 column and a P-E Nelson 1020 integrator were used along with a chemiluminescence NO_x analyzer (Thermo Environmental Instr. Inc., Model 42H) to differentiate between NO and NO_2 in the effluent [7]. The GC temperature program, i.e., hold at 228 K for 5 min, ramp at 35 K/min to 423 K, and hold for 5 min, provided good separation of N_2, O_2, NO, CO, CH_4, CO_2, N_2O, and H_2O, although the last peak was not quantifiable [7]. Unless otherwise specified, experiments in the presence of O_2 were performed with 25 mg of catalyst and a feed containing 1.4% NO, 0.35% CH_4, and 1.0% O_2 in He flowing at 45 cm^3 (STP)/min. The effects of CO_2 and H_2O were studied separately using standard concentrations of 9.0 and 2.0%, respectively. Distilled, deionized water was introduced to the reactor system via He flowing through a saturator held in a Neslab GP-100 constant temperature bath maintained between 305 and 325 K. The stainless steel tubing from the saturator to the reactor and all stainless steel lines downstream of the reactor were heated at 323 K to avoid water condensation. Before the reactor effluent entered the NO_x analyzer, it was diluted 10-fold with He. The gas mixtures used in the experiments were 4.03% NO in He, 9.80% O_2 in He, and 1.0% CH_4 in He, and they were prepared with gases from MG Ind. (99.999%, except for NO, which was 99.0+%). The CO_2 was also from MG Ind. (99.995%).

The standard catalyst pretreatment involved heating for 1 h at 973 K under 20 cm^3 (STP)/min of 10% O_2 in He. Following pretreatment the gas mixture was flowed for at least 30 min before any effluent stream analyses were conducted. NO reduction with CH_4 was performed between 773 and 973 K to obtain Arrhenius plots and to examine the effects of CO_2 and H_2O on apparent activation energies. A descending, then ascending temperature sequence was used to check for any deactivation. Activity versus time on stream was also monitored to determine both long-term and transient effects of CO_2 and H_2O in the feed stream on NO reduction. Partial pressure dependencies of activity on H_2O and CO_2 were determined at three or four different temperatures between 798 and 973 K by varying the inlet partial pressure of one reactant while keeping all other reactant concentrations and the total flow rate constant. The standard feed concentrations were 11 Torr NO (1.4%), 2.7 Torr CH_4 (0.35%), and 7.6 Torr O_2 (1.0%) in He. When the partial pressure of any of these three components was varied with either CO_2 or H_2O in the feed stream, the former was held at 68 Torr (9.0%) and the latter at 15 Torr (2.0%). NO was varied from 1.9 to 15 Torr (0.25–2.2%), CH_4 from 0.38 to 3.4 Torr (0.05–0.55%), O_2 from 1.9 to 22 Torr (0.35–1.8%), CO_2 from 8 to 130 Torr (1.0–17%), and H_2O from 2.3 to 22 Torr (0.3–3.0%).

3. Results

As observed with other La_2O_3-based catalysts [7,12], CO_2 reversibly inhibited the rate of NO reduction by CH_4 over supported La_2O_3 in either the absence or presence of

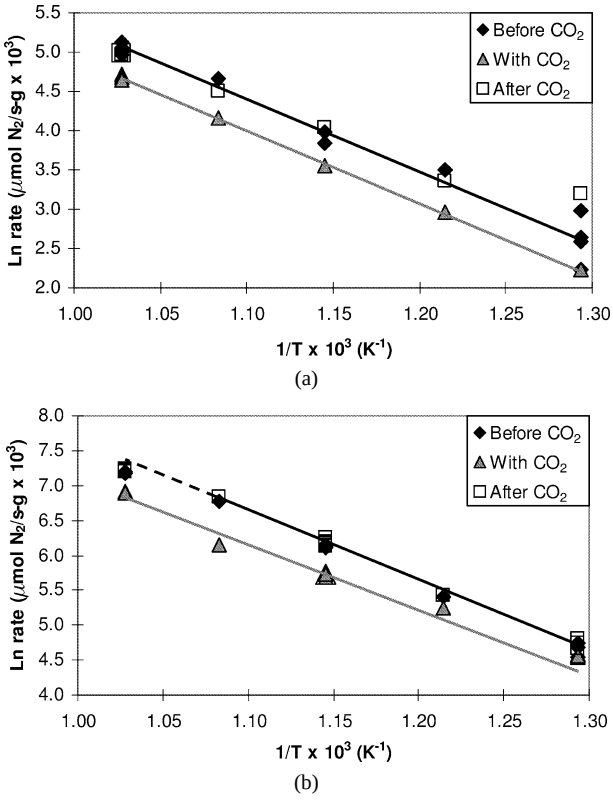

Fig. 1. Arrhenius plots characterizing the effect of CO_2 on NO reduction by CH_4 over 40% La_2O_3/γ-Al_2O_3 in (a) the absence of O_2 and (b) the presence of O_2. Reaction conditions: 1.4% NO, 0.35% CH_4, 0 or 1.0% O_2, 0 or 9.0% CO_2, balance He; GHSV = 60,000 h^{-1} in the absence of O_2 and 100,000 h^{-1} in the presence of O_2.

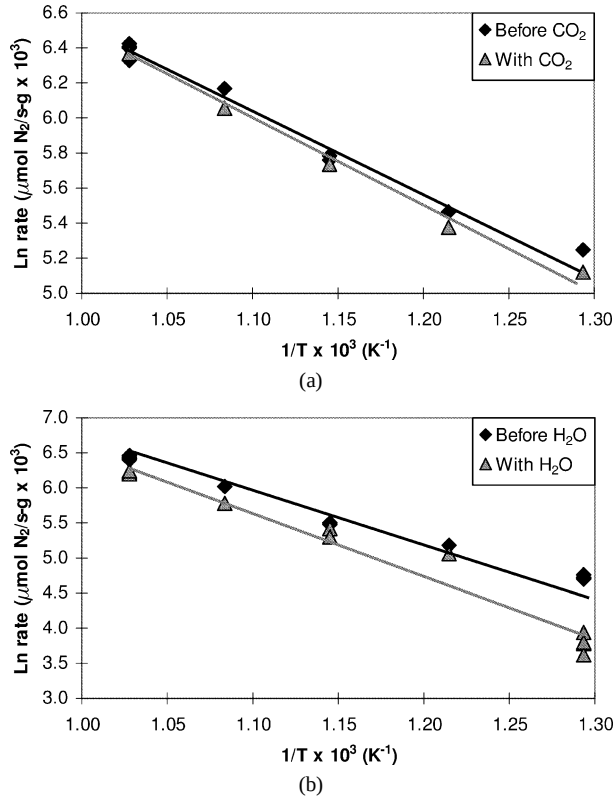

Fig. 2. Arrhenius plots for NO reduction by CH_4 over γ-Al_2O_3 in the presence of O_2 and with either (a) CO_2 or (b) H_2O in the feed. Reaction conditions: 1.4% NO, 0.35% CH_4, 1.0% O_2, 0 or 2.0% H_2O, balance He; GHSV = 87,000 h^{-1} with CO_2 in the feed and 110,000 h^{-1} with H_2O.

O_2; however, the inhibitory effect of CO_2 on the performance of the γ-Al_2O_3 alone was significantly smaller, especially in the presence of O_2 where virtually no decrease in activity was observed. Figs. 1–3 show the Arrhenius plots for 40% La_2O_3/Al_2O_3 and Al_2O_3, while the rates, specific activities, and apparent activation energies in the differential regime, in which all reactant conversions were less than 20% and which is depicted as a solid line in the Arrhenius plots, are reported in Tables 1 and 2. Each gas hourly space velocity (GHSV) was calculated using an approximate catalyst density of 1 g/cm^3. The effect of CO_2 was further examined by monitoring the activity versus time on stream to determine both the long term and the transient nature of the inhibition, as shown in Fig. 4 for La_2O_3/Al_2O_3 and Fig. 5 for Al_2O_3. With H_2O in the feed, a similar reversible effect on NO reduction was observed, as depicted by the Arrhenius plots in Fig. 6; however, unlike CO_2, water also caused considerable reversible inhibition of this reaction over Al_2O_3. The apparent activation energies, along with 90% probability limits, are reported in Table 1 for La_2O_3/Al_2O_3 and Table 2 for γ-Al_2O_3, and the activity vs time on stream results involving H_2O are displayed in Figs. 5, 7, and 8. In the absence of O_2, La_2O_3/γ-Al_2O_3 showed surprising behavior during time-on-stream runs when H_2O was added to and deleted from the feed (Fig. 8). While 1.4% NO and 0.35% CH_4 in He were flowed over this catalyst at 973 K, the initial activity increased slightly overnight (point A), as shown in Fig. 8a. Introducing steam into the feed decreased the activity overnight by about 50%, which is behavior consistent with that for unsupported La_2O_3 [7], but when steam was removed from the feed, the activity increased markedly to a value almost double the initial activity (point B). During the next 100 h on stream, the activity slowly declined to equal that during the initial period (point C). This result was investigated further using a modified reaction chamber so that any effects on surface area and NO uptakes could be monitored throughout this reaction sequence [7], and the kinetic sequence with H_2O was reproduced in this modified chamber, as shown in Fig. 8b. The corresponding NO isotherms at 300 K and surface areas measured at the labeled points, I, A, B, and C, are displayed in Fig. 9 and Table 3, respectively, along with the turnover frequency (TOF), which is normalized to the sites capable of irreversible NO adsorption at 300 K, i.e.,

$$\mathrm{TOF}[\mathrm{s}^{-1}] = \frac{\text{rate of } N_2 \text{ formation [mol/s g]}}{\text{irreversible NO uptake [mol/g]}}. \quad (1)$$

The relatively constant TOF values indicate that the change in activity can be attributed to a variation in the number of NO chemisorption sites due, most likely, to a change in the surface area of the La_2O_3 dispersed on the alumina surface.

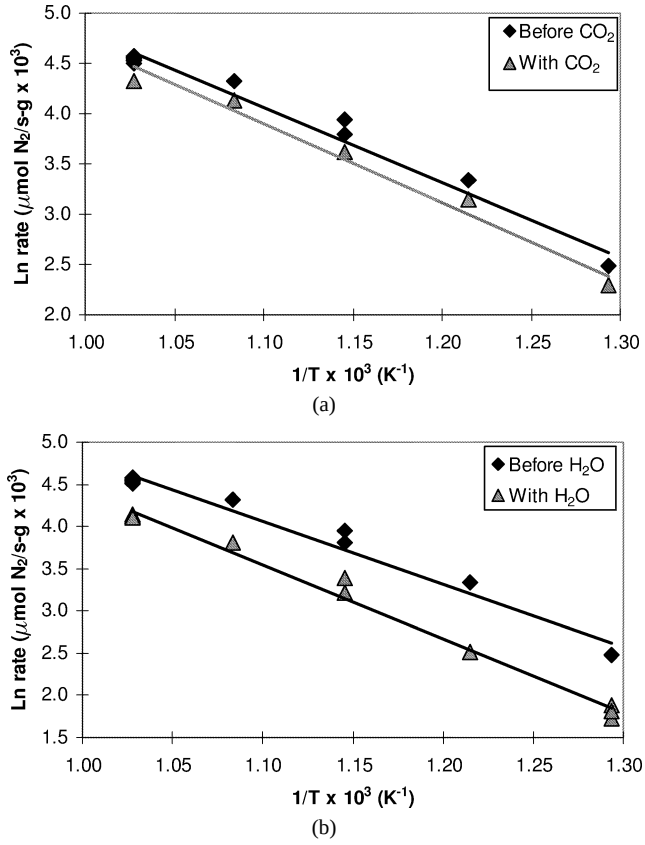

Fig. 3. Arrhenius plots for NO reduction by CH_4 over γ-Al_2O_3 in the absence of O_2 and with either (a) CO_2 or (b) H_2O in the feed. Reaction conditions: 1.4% NO, 0.35% CH_4, 0 or 9.0% CO_2, 0 or 2.0% H_2O; GHSV: 50,000 h^{-1}.

Reaction orders for this supported catalyst were determined in the absence of O_2 at four temperatures between 898 and 973 K following the procedure outlined earlier [7], and these results are tabulated in Table 4, while the experimental data are provided in Fig. 10 for CO_2 and Fig. 11 for H_2O. As expected with O_2 in the feed, direct combustion of CH_4 continued to be significant although NO conversions were kept below 20%; therefore, data analysis was conducted assuming integral reactor behavior [13,14]. These apparent reaction orders are also listed in Table 4, and the kinetic data are shown in Figs. 12 and 13.

XRD measurements were used to probe the effects of CO_2 and H_2O on the phases present in Al_2O_3-supported La_2O_3. As with unsupported La_2O_3 and Sr-promoted La_2O_3 [7,12], under reaction conditions with CO_2 in the feed, bulk transformation from La_2O_3 to an oxycarbonate (II-$La_2O_2CO_3$) phase occurred, as shown by the XRD patterns in Fig. 14. As with unsupported La_2O_3, the oxycarbonate phase disappeared after CO_2 was removed from the feed stream and the La_2O_3 phase was reestablished in either the presence or absence of O_2; however, a small remnant of the oxycarbonate phase (at $2\theta = 33.5°$) remained in the absence of O_2. After several experiments with the same sample, it became difficult to separate the catalyst from the quartz wool and a significant amount of quartz was detected by XRD as well, as indicated by the broad quartz peak at $2\theta = 25°$ in the pattern for regenerated La_2O_3 in Fig. 14b. With H_2O in the feed, no bulk phase transformation was observed, which is consistent with previous observations for La_2O_3 and Sr/La_2O_3 [7,12,16,17]. XRD patterns for pure γ-Al_2O_3 showed no change in the bulk-phase properties.

Table 1
Kinetic behavior with 40% La_2O_3/γ-Al_2O_3

	Rate (μmol N_2/s g × 10^3)		Specific activity (μmol N_2/s m^2 × 10^3)		E_a (kcal/mol)
	873 K	973 K	873 K	973 K	
9% CO_2 study					
O_2 absent					
Before CO_2	54	160	0.57	1.6	18 ± 2
With CO_2	9.3	110	0.10	1.1	18 ± 2
After CO_2	56	144	0.59	1.5	14 ± 3
O_2 present					
Before CO_2	470	1300	4.9	14	20 ± 2
With CO_2	300	990	3.2	10	17 ± 2
After CO_2	480	1400	5.2	15	20 ± 2
2% H_2O study					
O_2 absent					
Before H_2O	35	130	0.37	1.4	20 ± 2
With H_2O	17	73	0.17	0.80	25 ± 2
After H_2O	40	180	0.42	1.9	24 ± 2
O_2 present					
Before H_2O	750	1200	7.9	13	26 ± 4
With H_2O	416	940	4.4	9.9	31 ± 5
After H_2O	790	1100	8.3	12	24 ± 4

Reaction conditions: 1.4% NO, 0.35% CH_4, 0 or 1.0% O_2, 0 or 9.0% CO_2, 0 or 2% H_2O, balance He; GHSV = 60,000 h^{-1} in the absence of O_2 and 100,000 h^{-1} in the presence of O_2.

Table 2
Kinetic behavior for NO reduction by CH_4 over α-Al_2O_3

	Rate (μmol N_2/s g × 10^3)		Specific activity (μmol N_2/s m^2 × 10^3)		E_a (kcal/mol)
	873 K	973 K	873 K	973 K	
9% CO_2 study					
O_2 absent					
No CO_2	48	92	0.32	0.61	15 ± 3
With CO_2	37	74	0.25	0.49	16 ± 3
O_2 present					
No CO_2	330	610	2.2	4.1	8.8±2
With CO_2	320	600	2.1	4.0	9.5±2
2% H_2O study					
O_2 absent					
No H_2O	48	92	0.32	0.61	15±3
With H_2O	27	60	0.18	0.40	17±2
O_2 present					
No H_2O	247	611	1.6	4.1	13±2
With H_2O	224	507	1.5	3.4	17±4

Reaction conditions: 1.4% NO, 0.35% CH_4, 1.0% O_2, 0 or 9.0% CO_2, and 0 or 2% H_2O, balance He; GHSV = 85,000 h^{-1} with CO_2 in feed and 110,000 h^{-1} H_2O.

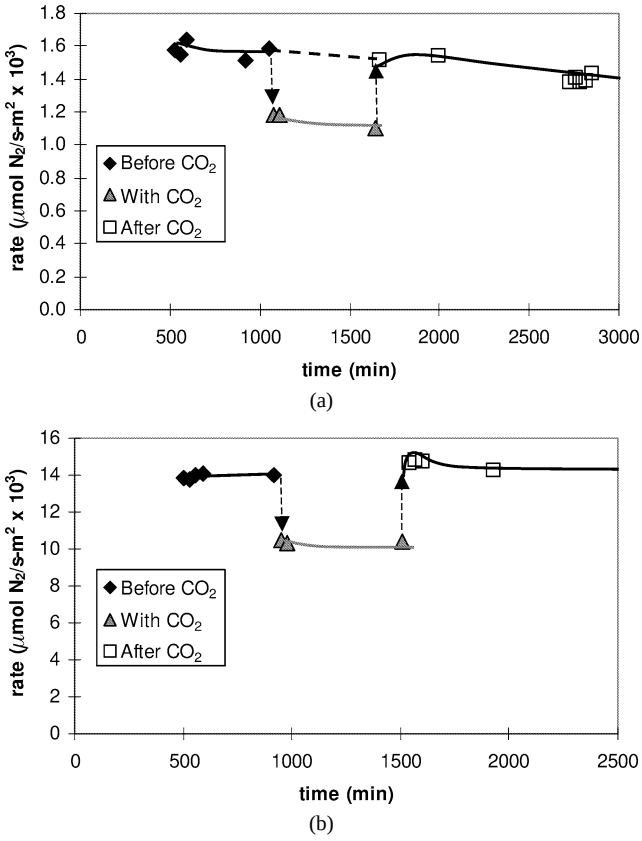

Fig. 4. Activity vs time on stream in the presence of CO_2 during NO reduction by CH_4 over 40% La_2O_3/γ-Al_2O_3 at 973 K (a) in the absence of O_2 and (b) in the presence of O_2. Reaction conditions: 1.4% NO, 0.35% CH_4, 0 or 1.0% O_2, and 0 or 9.0% CO_2, balance He; GHSV = 60,000 h^{-1} in the absence of O_2 and 100,000 h^{-1} in the presence of O_2.

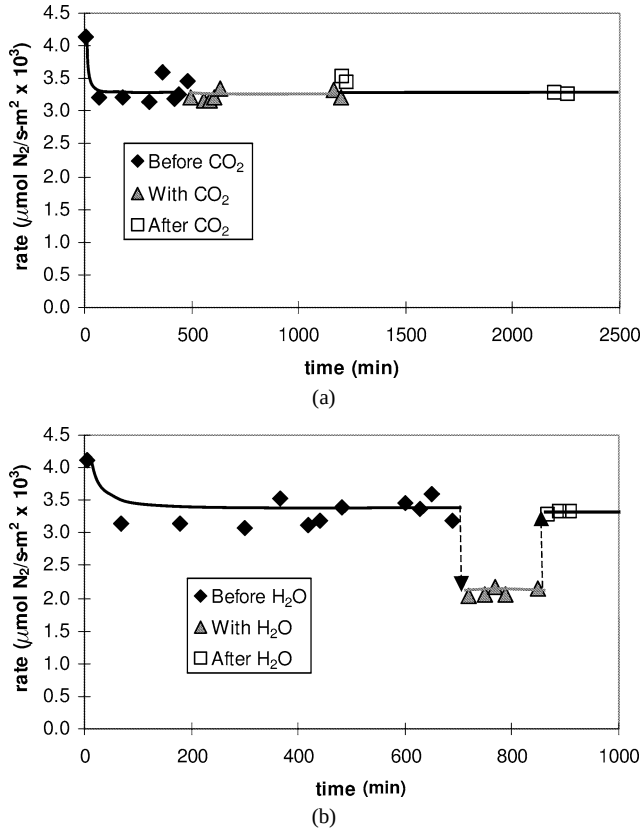

Fig. 5. Activity vs time on stream in the presence of O_2 during NO reduction by CH_4 over γ-Al_2O_3 at 973 K (a) in the presence of CO_2 and (b) in the presence of H_2O. Reaction conditions: 1.4% NO, 0.35% CH_4, 1.0% O_2, and either 0 or 9.0% CO_2 or 0 or 2% H_2O, balance He; GHSV = 85,000 h^{-1}.

4. Discussion

The rate inhibition on the 40% La_2O_3/γ-Al_2O_3 catalyst caused by CO_2 and H_2O was qualitatively the same as that observed with La_2O_3 and 4% Sr–La_2O_3 [7,12]; however, the degree of inhibition was considerably less with the supported catalyst. Either CO_2 or H_2O decreased the activity of unsupported La_2O_3 by around 75% in the absence of O_2 and about 50% in the presence of O_2, whereas the rate inhibition was only about 35% and 20%, respectively, for La_2O_3/Al_2O_3. This reduced degree of inhibition, especially in the presence of O_2, is a promising result because this supported system is the most industrially relevant of the La_2O_3-based catalysts investigated. When compared to the kinetic performance of other NO_x reduction catalysts that have been tested with H_2O in the feed [18–28], it is apparent that this is one of the most active catalysts for SCR of NO above 773 K with steam present, as indicated in Table 5. The TOFs for the La_2O_3/Al_2O_3 catalyst in this study were calculated from Eq. (1), but in the other studies, the rate was normalized to the concentration of metal cations in the catalyst, when possible. There is very limited information in the literature about the kinetic effects of CO_2 on oxide catalysts, as discussed more fully elsewhere [7].

The activity of alumina for NO reduction by CH_4 has been reported earlier [5], and while some studies have examined γ-Al_2O_3 as an NO_x reduction catalyst by itself, its primary utility has been as a support for more active catalysts. It is an attractive support because of its strong thermal stability in oxidizing environments [8–11]; however, as mentioned earlier, steam can facilitate sintering in transitional aluminas. The temperatures were low enough in this study so that no significant sintering was observed with either pure Al_2O_3 or Al_2O_3-supported La_2O_3. Coincidentally, La_2O_3 has been used to inhibit steam-induced sintering of alumina [29–32], so the presence of La_2O_3 may stabilize its surface at higher temperatures.

It is clear from the kinetic results provided in Tables 1 and 2 that γ-Al_2O_3 can make a significant contribution to NO reduction activity, especially in the presence of CO_2 and H_2O, and the results in Fig. 8 suggest that there may be a synergistic effect as well. The large increase in activity after removal of H_2O from the feed was unique to this catalyst and was observed only in the absence of O_2. From the chemisorption results reported in Table 3, it is clear that the surface has a substantially higher concentration of NO adsorption sites after exposure to H_2O; however, this concentration decreases with time and reaches the original

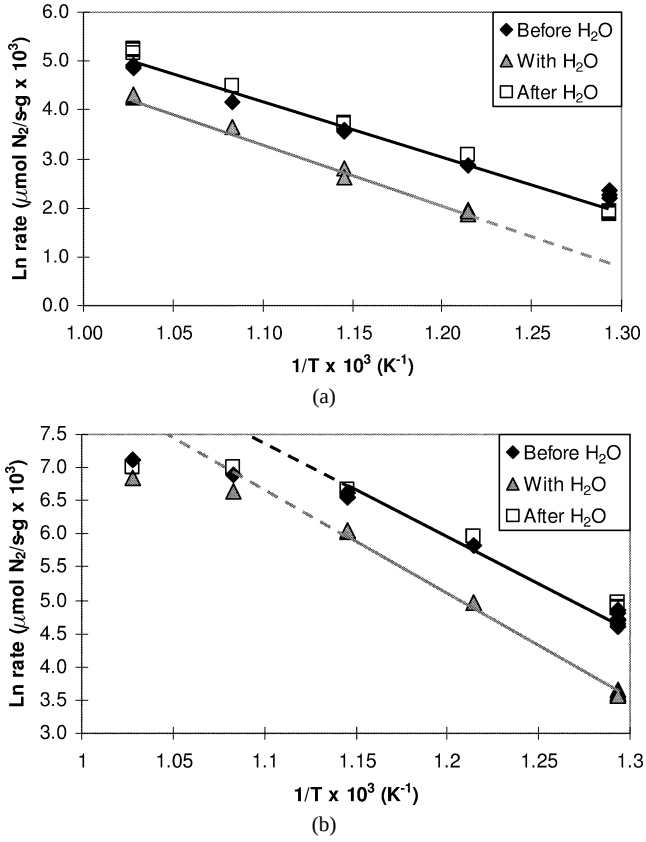

Fig. 6. Arrhenius plot characterizing the effect of H_2O on NO reduction by CH_4 over 40% La_2O_3/γ-Al_2O_3 in (a) the absence of O_2 and (b) the presence of O_2. Reaction conditions: 1.4% NO, 0.35% CH_4, 0 or 1.0% O_2, 0 or 2.0% H_2O, balance He; GHSV = 60,000 h^{-1} in the presence of O_2 and 100,000 h^{-1} in the absence of O_2.

level about 50 h after the removal of water from the feed. This behavior is quite reproducible and is most likely due to a La_2O_3 redispersion effect that occurs in the absence of O_2, but not with O_2 in the feed. However, another explanation for this behavior is possible. The results in this study show that the activity doubles only in the absence of O_2 with H_2O present and that under these conditions the

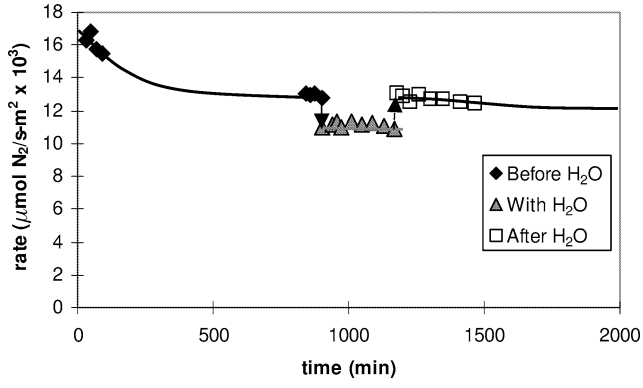

Fig. 7. Activity vs time on stream in the presence of H_2O during NO reduction by CH_4 40% La_2O_3/γ-Al_2O_3 at 973 K in the presence of O_2. Reaction conditions: 1.4% NO, 0.35% CH_4, 1.0% O_2, and 0 or 2.0% H_2O, balance He; GHSV = 108,000 h^{-1}.

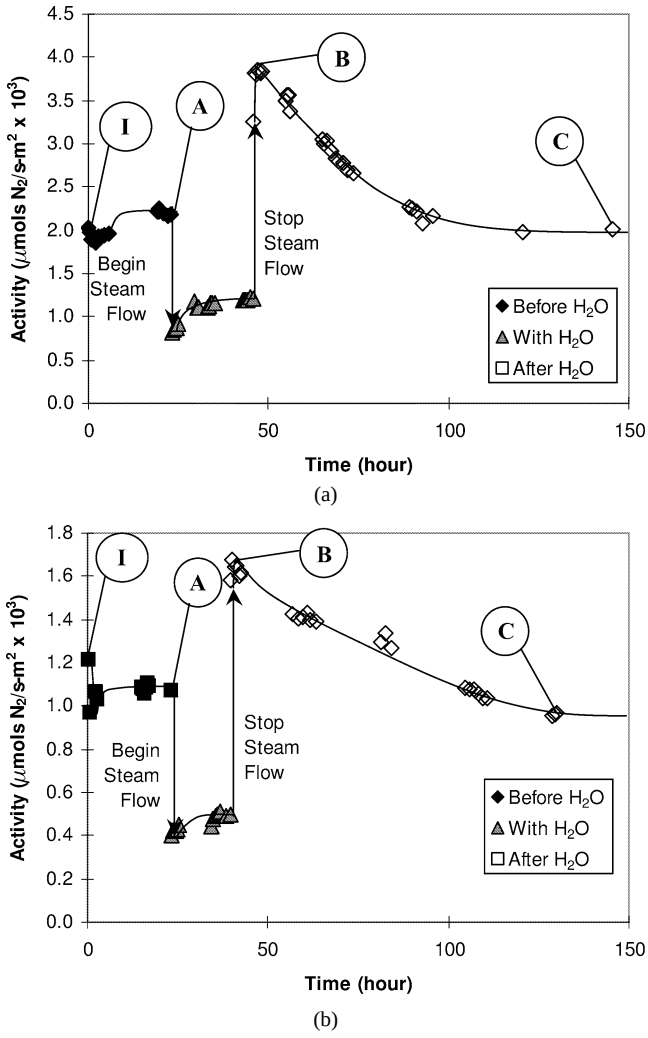

Fig. 8. Time on stream study of the effect of steam on NO reduction by CH_4 over 40% La_2O_3/γ-Al_2O_3 at 973 K (a) in the microreactor with GHSV = 56,000 h^{-1} and (b) in the chemisorption system with GHSV = 36,000 h^{-1}. Reaction conditions: 1.4% NO, 0.35% CH_4, 0% O_2, 0 or 2.0% H_2O, balance He.

reaction orders on NO increase to near unity, which suggests a lower surface coverage of NO. Earlier experiments have shown that: (a) La_2O_3 is susceptible to the loss of surface lattice oxygen [6]; (b) the concentration of surface oxygen vacancies positively affects the NO adsorption behavior [6,33]; (c) NO adsorption is aided by surface O–S groups [6]; and (d) H_2O can create OH^- species on high surface area alumina surfaces [10,34]. With these aspects in mind, it may be that when H_2O was removed from the feed, the high concentration of OH^- groups on the Al_2O_3 surface, which were equilibrated with gas-phase H_2O, decreases due to dehydroxylation and generates surface oxygen sites, as shown in the equation

$$2\text{OH–S} \not\rightleftharpoons \text{O–S} + \text{H}_2\text{O–S}, \tag{2}$$

which would increase the concentration of NO adsorption sites after H_2O desorption as shown below (Eq. (8)).

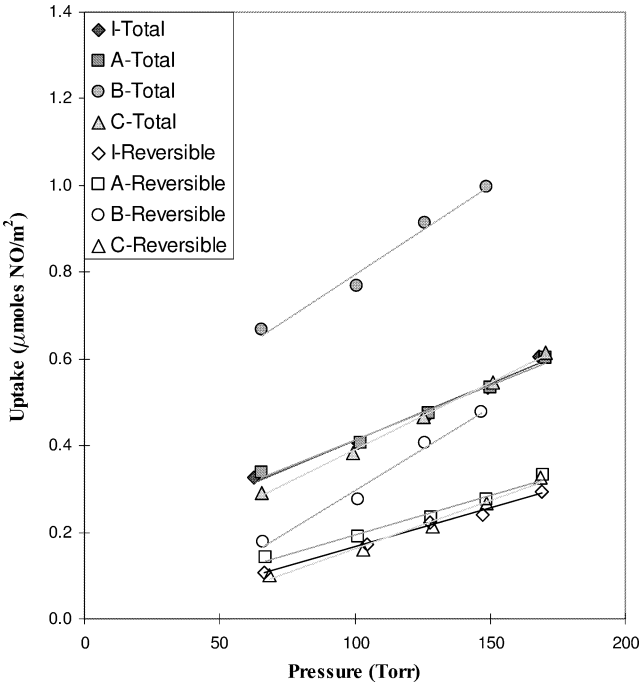

Fig. 9. NO chemisorption at 300 K on 40% La_2O_3/γ-Al_2O_3 after reaction at points noted in Fig. 7. Reaction conditions: $T = 973$ K, GHSV = 36,000 h^{-1}, and 1.4% NO, 0.35% CH_4, 0% O_2, 0 or 2% H_2O, balance He.

Despite this behavior, one can begin by assuming that the reaction mechanisms and rate laws proposed earlier for unsupported La_2O_3 remain applicable for La_2O_3 dispersed on alumina [35]. The effects of CO_2 and H_2O can be easily incorporated into the kinetic rate expression by assuming that these two products compete for adsorption on the active sites. A detailed reaction mechanism in the absence of O_2 has been proposed previously [7], and only a shortened form containing the kinetically significant steps for NO reduction by CH_4 is shown below,

$$4\left[\mathrm{NO} + \mathrm{S} \overset{K_{\mathrm{NO}}}{\leftrightarrows} \mathrm{NO\text{–}S}\right] \tag{3}$$

$$\mathrm{CH_4} + \mathrm{S} \overset{K_{\mathrm{CH_4}}}{\leftrightarrows} \mathrm{CH_4\text{–}S} \tag{4}$$

$$\mathrm{NO\text{–}S} + \mathrm{CH_4\text{–}S} \overset{k}{\rightarrow} \mathrm{HNO\text{–}S} + \mathrm{CH_3\text{–}S} \quad \text{(rds)} \tag{5}$$

$$3\mathrm{NO\text{–}S} + \mathrm{HNO\text{–}S} + \mathrm{CH_3\text{–}S} \overset{K}{\leftrightarrows} 2\mathrm{H_2O\text{–}S} + 2\mathrm{N_2} + \mathrm{CO_2\text{–}S} + 2\mathrm{S} \tag{6}$$

$$\mathrm{CO_2\text{–}S} \overset{1/K_{\mathrm{CO_2}}}{\leftrightarrows} \mathrm{CO_2} + \mathrm{S} \tag{7}$$

$$2\left[\mathrm{H_2O\text{–}S} \overset{1/K_{\mathrm{H_2O}}}{\leftrightarrows} \mathrm{H_2O} + \mathrm{S}\right] \tag{8}$$

$$4\mathrm{NO} + \mathrm{CH_4} \rightarrow 2\mathrm{N_2} + 2\mathrm{H_2O} + \mathrm{CO_2}, \tag{9}$$

where reaction (5) is the rate-determining step (rds) and K_i represent adsorption equilibrium constants. If adsorbed CH_4, NO, and H_2O constitute the principal surface intermediates, so that the resulting site balance for total active site concentration, L, is $L = [\mathrm{CH_4\text{–}S}] + [\mathrm{NO\text{–}S}] + [\mathrm{CO_2\text{–}S}] + [\mathrm{H_2O\text{–}S}] + [\mathrm{S}]$, the following rate expression for N_2 formation is derived [14],

$$r_{\mathrm{N_2}} = k'_{\mathrm{NO}} P_{\mathrm{NO}} P_{\mathrm{CH_4}} \times (1 + K_{\mathrm{NO}} P_{\mathrm{NO}} + K_{\mathrm{CH_4}} P_{\mathrm{CH_4}} + K_{\mathrm{CO_2}} P_{\mathrm{CO_2}} + K_{\mathrm{H_2O}} P_{\mathrm{H_2O}})^{-2}, \tag{10}$$

Table 4
Reaction orders for the reduction of NO by CH_4 over 40% La_2O_3/γ-Al_2O_3 with CO_2 or H_2O in the feed

	NO	CH_4	O_2	CO_2	H_2O
			CO_2 study		
O_2 absent					
973 K	0.52	0.31	–	−0.10	–
948 K	0.43	0.33	–	−0.10	–
923 K	0.44	0.30	–	−0.10	–
O_2 present					
923 K	0.89	0.20	0.54	−0.07	–
898 K	0.82	0.23	0.53	−0.03	–
873 K	0.92	0.29	0.37	−0.04	–
			H_2O study		
O_2 absent					
973 K	0.97	0.32	–	–	−0.29
948 K	0.89	0.28	–	–	−0.19
923 K	0.96	0.26	–	–	−0.20
898 K	1.07	0.21	–	–	−0.22
O_2 present					
873 K	0.59	0.84	0.08	–	−0.22
848 K	0.47	1.14	−0.01	–	−0.19
823 K	0.45	0.95	0.06	–	−0.32
798 K	0.57	0.66	0.08	–	−0.16

Reaction conditions: 1.4% NO, 0.35% CH_4, 0 or 1.0% O_2, 0 or 9.0% CO_2, 0 or 2.0% H_2O, balance He; GHSV = 20,000–50,000 h^{-1} in the absence of O_2 and 90,000–100,000 h^{-1} in the presence of O_2.

Table 3
Kinetic parameters at various times on stream noted in Fig. 7b during NO reduction by CH_4 over 40% La_2O_3/γ-Al_2O_3

	Rate (μmol N_2/s g)	Surface area (m^2/g)	Specific activity (μmol N^2/s m^2 × 10^3)	NO uptake (μmol NO/g)	TOF[a] (s^{-1} × 10^3)
Initial rate(I)	0.120	97	1.2	17	7.0
Before H_2O(A)	0.100	93	1.1	15	6.7
H_2O effect (B)	0.160	93	1.7	23	6.9
After H_2O(C)	0.090	93	1.0	15	6.1

Reaction conditions: 1.4% NO, 0.35% CH_4, 0 or 2.0% H_2O, balance He; GHSV = 36,000 h^{-1}.
[a] TOF defined as μmol N_2/s/μmol NO_{ad}.

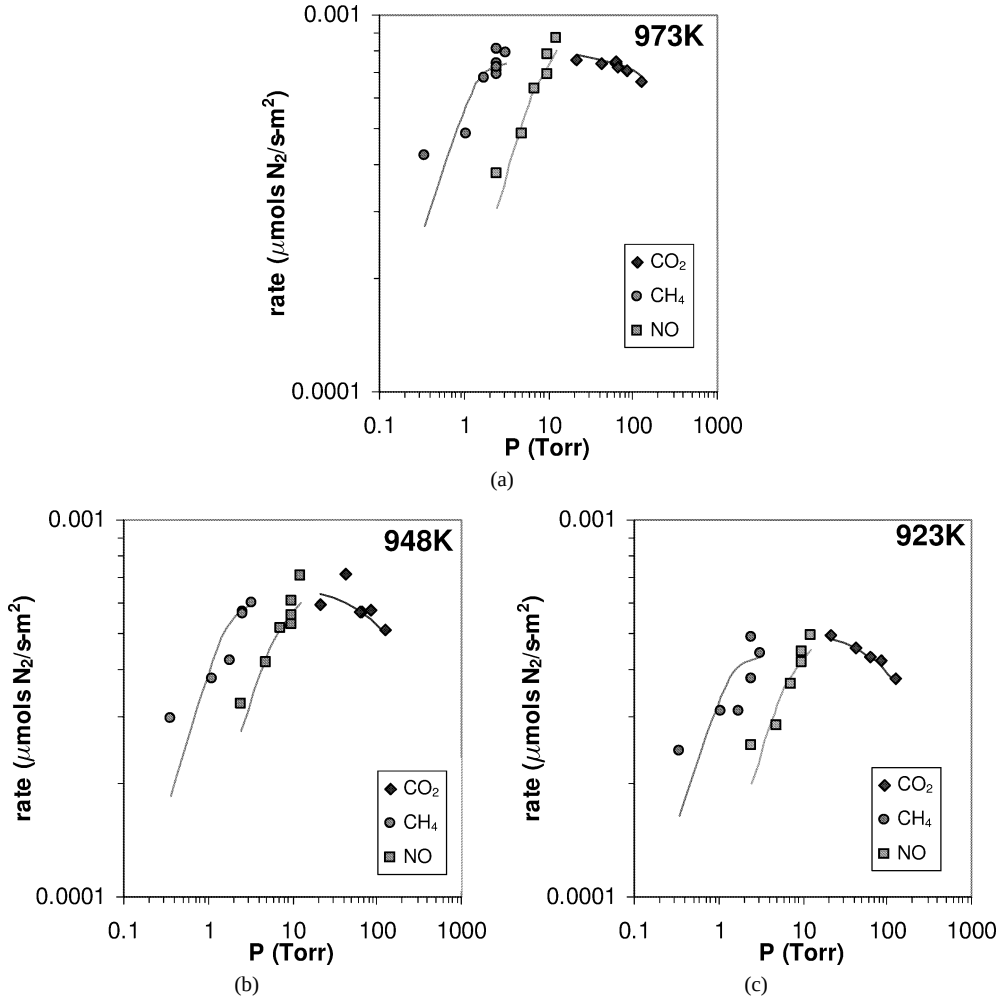

Fig. 10. Partial pressure dependencies for NO reduction by CH_4 over 40% La_2O_3/γ-Al_2O_3 in the absence of O_2 but with CO_2 in the feed at (a) 973 K, (b) 948 K, and (c) 923 K. Experimental data are represented by symbols and the rate expression given by Eq. (10) is represented by lines. Reaction conditions: 1.4% NO, 0.35% CH_4, and 9% CO_2, balance He; GHSV = 20,000 h^{-1}.

where $k'_{NO} = LkK_{NO}K_{CH_4}$. As with La_2O_3, differential reactor conditions were maintained throughout the experiments in the absence of O_2 and a straightforward optimization routine could be used to determine the fitting parameters [7,13,14]. The capability of this equation to fit the data is satisfactory and is represented as solid lines in Figs. 10 and 11 for CO_2 and H_2O, respectively, while the optimized fitting parameters at each temperature are listed in Table 6. The results indicate that surface coverage of oxygen and water are negligible with CO_2 in the feed, while coverages of NO, oxygen, and CO_2 are very low with H_2O in the feed and can be neglected in the site balance. All but one of these fitting parameters represent equilibrium adsorption constants, so they were further examined for thermodynamic consistency [14]. The entropies and enthalpies of adsorption derived from these constants are listed in Table 7 along with 90% confidence limits, and they were analyzed based on criteria discussed elsewhere to verify they are thermodynamically meaningful [36,37]. These values are also quite consistent with those reported for La_2O_3 under similar conditions [7]. The activation energy for the rate constant k in the rate-determining step to form a methyl group (Eq. (5)) was 25 ± 9 kcal/mol with CO_2 in the feed, but it could not be determined in the H_2O study because the $K_{NO}P_{NO}$ term essentially went to zero.

As discussed elsewhere for La_2O_3 and Sr-promoted La_2O_3 [7,12], both the surface chemistry and the subsequent data analysis become much more complex under lean-burn conditions in the presence of O_2, and here it is even more difficult because Al_2O_3 can also contribute to the kinetics of CH_4 combustion. Both La_2O_3 and Al_2O_3 catalyze the direct oxidation of CH_4 with O_2, as shown elsewhere [13]; consequently, differential reactor conditions could not be maintained for all reactants at all conditions. Even though NO conversion was always less than 20%, total methane and oxygen conversions were around 50% at times; thus rate data were analyzed assuming an integral reactor design equation to describe the concentration profiles throughout the catalyst bed [13,14]. The rate expressions for both the NO reduction reaction and the CH_4 combustion

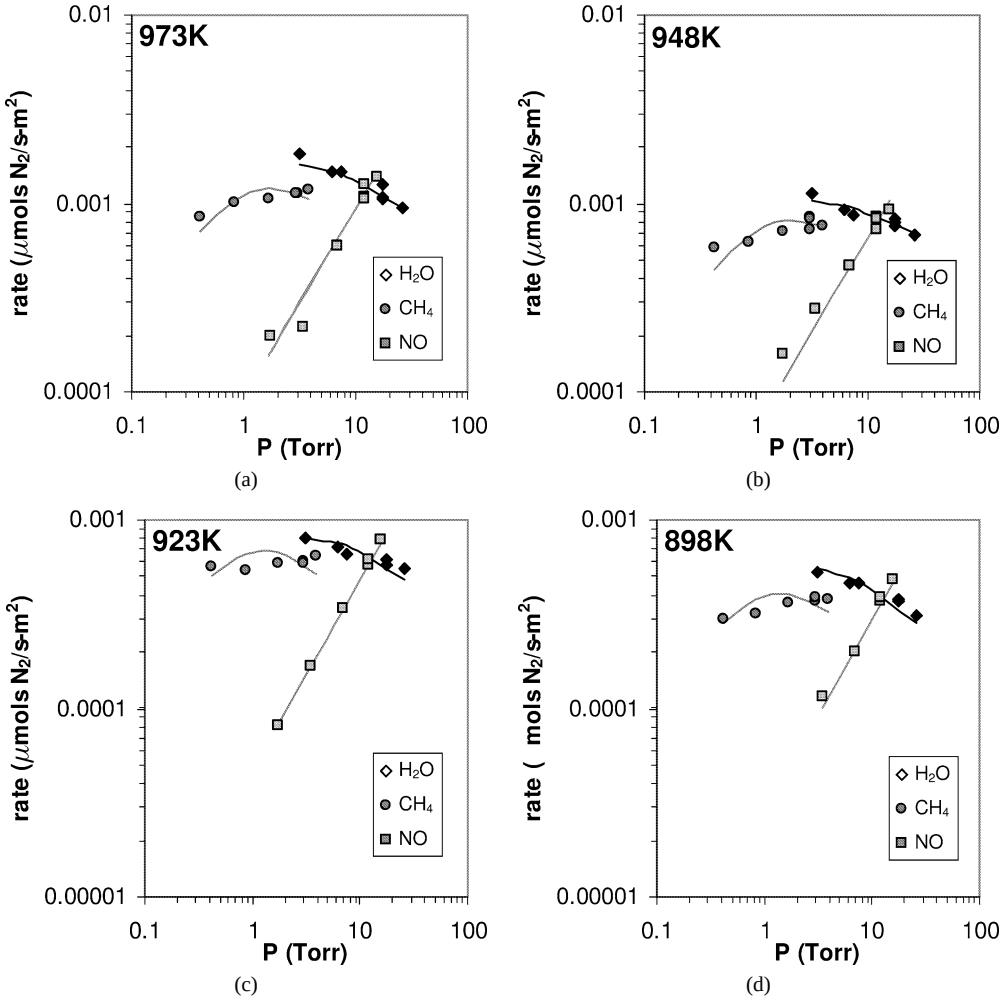

Fig. 11. Partial pressure dependencies for NO reduction by CH_4 over 40% La_2O_3/γ-Al_2O_3 in the absence of O_2 but with H_2O in the feed at (a) 973 K, (b) 948 K, (c) 923 K, and (d) 898 K. Experimental data are represented by symbols and the rate expression given by Eq. (10) is represented by lines. Reaction conditions: 1.4% NO, 0.35% CH_4, and 2.0% H_2O, balance He; GHSV = 50,000 h^{-1}.

reaction were simultaneously utilized to calculate reactant concentrations throughout the catalyst bed and to optimize the fitting parameters in these two rate equations [13,14].

It is again assumed that the surface chemistry and reaction mechanism are the same for both supported and unsupported La_2O_3 and, if so, after the inclusion of molecular CO_2 and H_2O adsorption the abbreviated mechanism with all kinetically significant steps is [7,35]

$$4\left[\mathrm{NO} + \mathrm{S} \overset{K_{\mathrm{NO}}}{\leftrightarrows} \mathrm{NO\text{–}S}\right] \tag{11}$$

$$2\left[\mathrm{CH_4} + \mathrm{S} \overset{K_{\mathrm{CH_4}}}{\leftrightarrows} \mathrm{CH_4\text{–}S}\right] \tag{12}$$

$$2\left[\mathrm{O_2} + 2\mathrm{S} \overset{K_{\mathrm{O_2}}}{\leftrightarrows} 2\mathrm{O\text{–}S}\right] \tag{13}$$

$$3\left[\mathrm{NO\text{–}S} + \mathrm{O\text{–}S} \overset{K_{\mathrm{NO_2}}}{\leftrightarrows} \mathrm{NO_2\text{–}S} + \mathrm{S}\right] \tag{14}$$

$$2\left[\mathrm{NO_2\text{–}S} + \mathrm{CH_4\text{–}S} \overset{k}{\rightarrow} \mathrm{HNO_2\text{–}S} + \mathrm{CH_3\text{–}S}\right] \quad \text{(rds)} \tag{15}$$

$$2\mathrm{HNO_2\text{–}S} + 2\mathrm{CH_3\text{–}S} + \mathrm{NO\text{–}S} + \mathrm{NO_2\text{–}S} + \mathrm{O\text{–}S} \overset{K}{\leftrightarrows} 2\mathrm{CO_2\text{–}S} + 4\mathrm{H_2O\text{–}S} + 2\mathrm{N_2} + \mathrm{S} \tag{16}$$

$$2\left[\mathrm{CO_2\text{–}S} \overset{1/K_{\mathrm{CO_2}}}{\leftrightarrows} \mathrm{CO_2} + \mathrm{S}\right] \tag{17}$$

$$4\left[\mathrm{H_2O\text{–}S} \overset{1/K_{\mathrm{H_2O}}}{\leftrightarrows} \mathrm{H_2O} + \mathrm{S}\right] \tag{18}$$

$$4\mathrm{NO} + 2\mathrm{CH_4} + \mathrm{O_2} \rightarrow 2\mathrm{N_2} + 4\mathrm{H_2O} + 2\mathrm{CO_2}. \tag{19}$$

With reaction (15) as the rds and CH_4–S, NO–S, O–S, CO_2–S, and H_2O–S as the principal surface species in the site balance, the derived rate expression for N_2 formation is

$$r_{\mathrm{N_2}} = \left(Lk K_{\mathrm{NO_2}} K_{\mathrm{NO}} K_{\mathrm{CH_4}} K_{\mathrm{O_2}}^{0.5}\right) P_{\mathrm{NO}} P_{\mathrm{CH_4}} P_{\mathrm{O_2}}^{0.5} \times \left(1 + K_{\mathrm{NO}} P_{\mathrm{NO}} + K_{\mathrm{CH_4}} P_{\mathrm{CH_4}} + K_{\mathrm{CO_2}} P_{\mathrm{CO_2}} + K_{\mathrm{H_2O}} P_{\mathrm{H_2O}} + K_{\mathrm{O_2}}^{0.5} P_{\mathrm{O_2}}^{0.5}\right)^{-2}. \tag{20}$$

Based on the stoichiometry in Eq. (19), this expression relates directly to CH_4 disappearance due to NO reduction because $r_{\mathrm{N_2}} = (r_{\mathrm{CH_4}})_{\mathrm{NO}} = \mathrm{d[N_2]}/\mathrm{d}t = -\mathrm{d[CH_4]}/\mathrm{d}t$. This rate expression can be combined with that for CH_4 disappearance

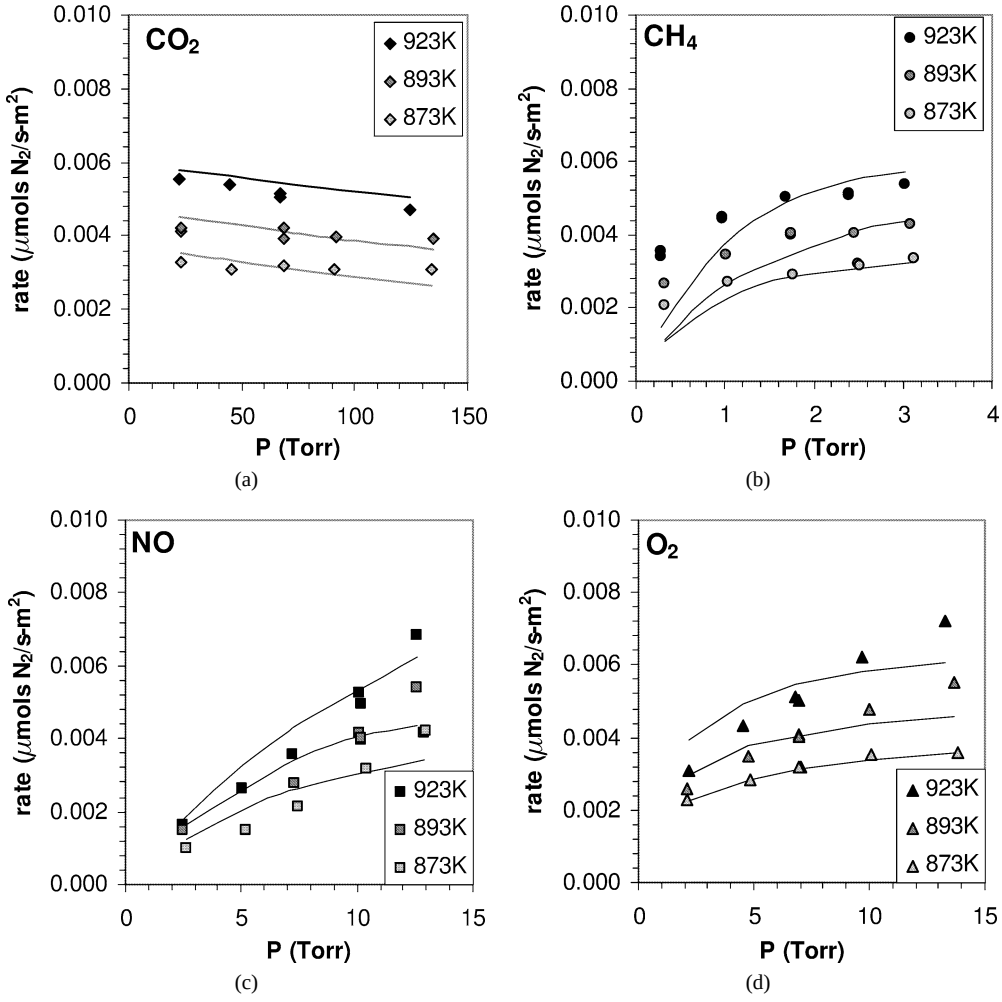

Fig. 12. Partial pressure dependencies for NO reduction by CH_4 over 40% La_2O_3/γ-Al_2O_3 with O_2 and CO_2 in the feed: (a) CO_2, (b) CH_4, (c) NO, and (d) O_2. Experimental data are represented by symbols and the rate expression given by Eq. (24) is represented by lines. Reaction conditions: 1.4% NO, 0.35% CH_4, 1.0% O_2, and 9% CO_2, balance He; GHSV = 90,000 h^{-1}.

due to direct oxidation [13] to give the rate of total methane disappearance,

$$(r_{CH_4})_T = \left(k'_{com} P_{CH_4} P_{O_2}^{0.5} + k'_{NO} P_{NO} P_{CH_4} P_{O_2}^{0.5}\right) \times \left(1 + K_{NO} P_{NO} + K_{CH_4} P_{CH_4} + K_{O_2}^{0.5} P_{O_2}^{0.5} + K_{CO_2} P_{CO_2} + K_{H_2O} P_{H_2O}\right)^{-2}, \quad (21)$$

where $k'_{com} = Lk' K_{CH_4} K_{O_2}^{0.5}$ and $k'_{NO} = Lk K_{NO_2} K_{NO} \times K_{CH_4} K_{O_2}^{0.5}$ [7,14]. The partial pressure of each component can be quantitatively related to P_{CH_4}, and a commercial optimization program (Scientist 2.01, Micromath Sci. Software) was used to obtain the fitting parameters in this complex rate expression, assuming integral reactor behavior to calculate concentration gradients and evaluate performance, as described elsewhere [7,13,14].

In the presence of H_2O this rate law provided a very good fit, as shown in Fig. 13, and the optimized rate constants are listed in Table 6, while the thermodynamic parameters are given in Table 7. Due to the inclusion of K_{NO_2} in the lumped rate constant, it was not possible to calculate the activation energy for the rds described by Eq. (15). With CO_2 in the feed this rate expression could fit the experimental data satisfactorily but, in contrast, some of the enthalpies and entropies were thermodynamically inconsistent [14,36,37], so this model had to be rejected and other alternatives considered. Because CO_2 had little effect on the SCR of NO over γ-Al_2O_3 with O_2 present, as shown in Fig. 2, it is hypothesized that the contribution from Al_2O_3 became increasingly significant as CO_2 suppressed the rate on La_2O_3, thus explaining the inconsistent thermodynamic behavior. This inhibition by CO_2 may well be due to the formation of a bulk lanthanum oxycarbonate, $La_2O_2CO_3$, which can form if CO_2 concentrations are high enough [7]. Fig. 14 verifies that $La_2O_2CO_3$ was indeed present.

A partial pressure study was then conducted with γ-Al_2O_3 to determine a rate law describing the kinetic behavior of NO reduction by CH_4, and the experimental data are displayed in Fig. 15 while reaction orders are listed in Table 8. Eq. (21) proved to be unsuccessful both in terms of quality of fit and in thermodynamic consistency, and the

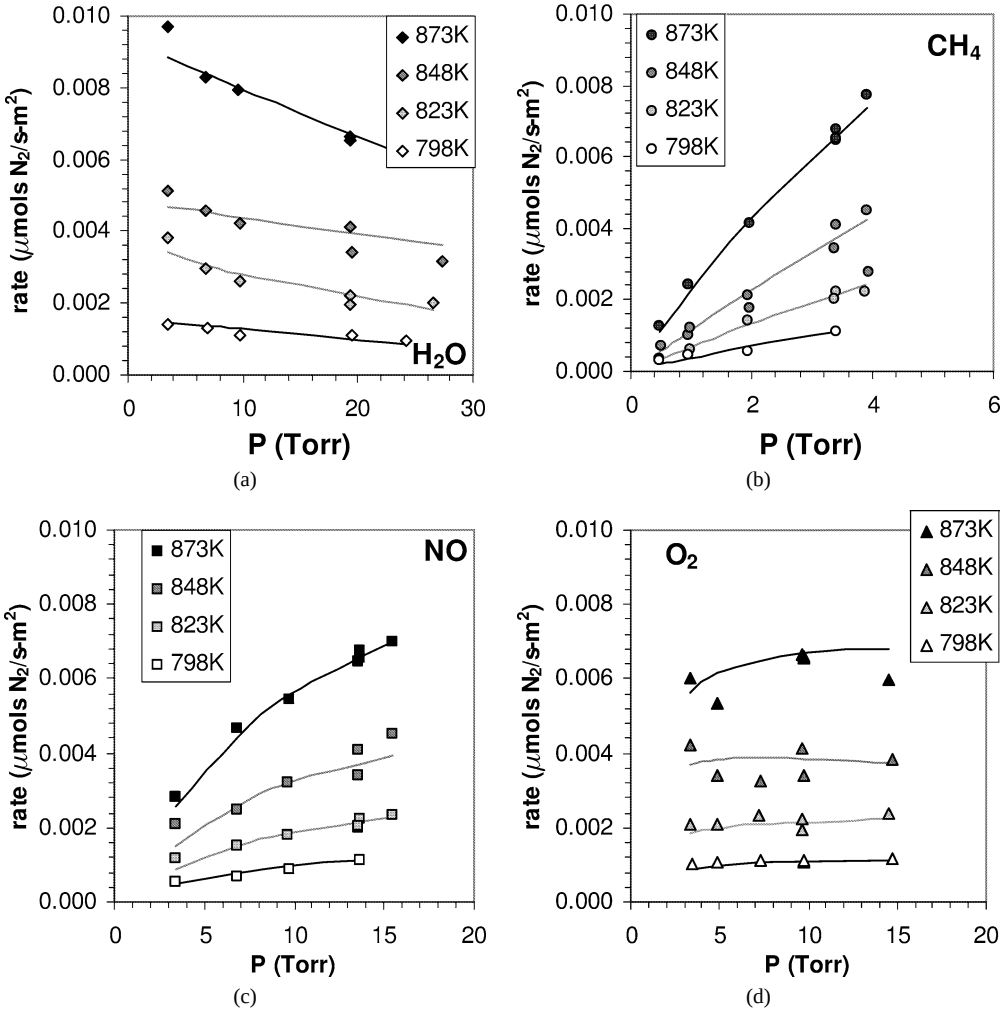

Fig. 13. Partial pressure dependencies for NO reduction by CH_4 over 40% La_2O_3/γ-Al_2O_3 with O_2 and H_2O in the feed: (a) H_2O, (b) CH_4, (c) NO, and (d) O_2. Experimental data are represented by symbols and the rate expression given by Eq. (23) is represented by lines. Reaction conditions: 1.4% NO, 0.35% CH_4, 1.0% O_2, and 2.0% H_2O, balance He; GHSV = 100,000 h^{-1}.

fit was especially poor with respect to the NO partial pressure, suggesting that a different N-containing intermediate may predominate on the surface of γ-Al_2O_3. Studies of NO on alumina have suggested that NO_2 species may have strong interactions with the γ-Al_2O_3 surface [6,38]; thus, one might propose that adsorbed NO_2, rather than NO, is the most abundant N-containing species. With this and the same earlier assumptions about other surface species, the rate law can be derived for N_2 formation on γ-Al_2O_3 [14],

$$r_{N_2} = \left(Lk K_{NO_2} K_{NO} K_{CH_4} K_{O_2}^{0.5}\right) P_{NO} P_{CH_4} P_{O_2}^{0.5} \times \left(1 + K'_{NO_2} P_{NO} P_{O_2}^{0.5} + K_{CH_4} P_{CH_4} + K_{CO_2} P_{CO_2} + K_{H_2O} P_{H_2O} + K_{O_2}^{0.5} P_{O_2}^{0.5}\right)^{-2}, \quad (22)$$

where $K'_{NO_2} = K_{NO_2} K_{NO} K_{O_2}^{0.5}$. This can be combined with the combustion rate expression [13] to yield the rate equation for total CH_4 disappearance over just the Al_2O_3 surface,

$$(r_{CH_4})_T = \left(k'_{com} P_{CH_4} P_{O_2}^{0.5} + k'_{NO} P_{NO} P_{CH_4} P_{O_2}^{0.5}\right) \times \left(1 + K'_{NO_2} P_{NO} P_{O_2}^{0.5} + K_{CH_4} P_{CH_4} + K_{O_2}^{0.5} P_{O_2}^{0.5} + K_{CO_2} P_{CO_2} + K_{H_2O} P_{H_2O}\right)^{-2}, \quad (23)$$

where $k'_{com} = Lk' K_{CH_4} K_{O_2}^{0.5}$ and $k'_{NO} = Lk K_{NO_2} K_{NO} \times K_{CH_4} K_{O_2}^{0.5}$. This rate law provided a good fit for the data with alumina, as depicted by the lines in Fig. 15, and the optimized rate constants are listed in Table 6 along with their units. Tests for thermodynamic consistency were limited to just the CH_4 equilibrium adsorption constant because the optimization routine returned zero values for $K_{O_2} P_{O_2}$ and $K_{CO_2} P_{CO_2}$ ($K_{H_2O} P_{H_2O}$ was not varied), and this indicated a somewhat higher heat of adsorption for CH_4 on alumina of 32 kcal/mol.

At this point it is perhaps appropriate to assess the implications of the values listed in Table 7 and to determine what can be said about the nature of the active sites on a lanthana surface. The heats of adsorption (and entropies) obtained from the fitting parameters for NO, O_2, CO_2, and H_2O on a lanthana surface are reasonable, although no experimental values exist for comparison, but the heats of adsorption indicated for CH_4 are far too large for nondissociative adsorp-

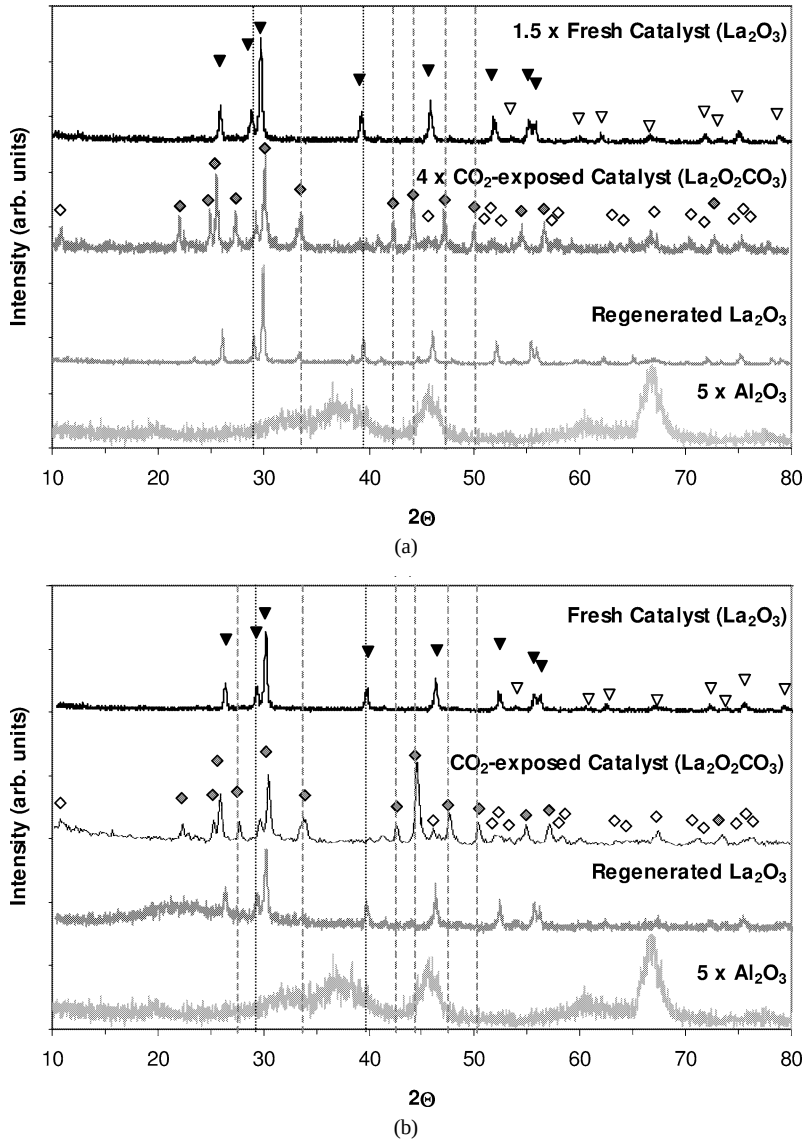

Fig. 14. XRD patterns characterizing the effects of CO_2 on the phases present in 40% La_2O_3/γ-Al_2O_3 (a) in the absence of O_2 and (b) in the presence of O_2. Lines represent unique peaks for La_2O_3 (···) and $La_2O_2CO_3$ (–). Symbols represent characteristic peaks for La_2O_3 (▼, ▽) and II-$La_2O_2CO_3$ (♦, ◊), with filled symbols representing principal peaks.

tion. Consequently, dissociative adsorption is implied, either homolytic or heterolytic, but it occurs at a single "site" to be consistent with our model. Theoretical calculations of heterolytic CH_4 adsorption on La_2O_3 and Al_2O_3 by Capitan et al. have indicated heats of adsorption of 18–21 kcal/mol on a lanthana surface and 22–28 kcal/mol on an alumina surface [39]. Not only are these values quite close to those in Table 7, but that calculated for alumina is also larger, again consistent with Table 7. Earlier calculations by Ito et al. estimated a heat of adsorption for CH_4 on MgO of 23 kcal/mol for heterolytic adsorption on a coordinatively unsaturated (cus) Mg^{2+}–O^{2-} site pair [40]. A detailed discussion of the sites that can exist on a lanthana surface has recently been provided and various types of oxygen vacancies were identified [41]. An oxygen vacancy would constitute a cus site, and the possibility that this could be an active site, especially since NO and O_2 adsorption can also occur on such a site, has been considered elsewhere [6]. Thus, one reasonable modification of the original models shown in steps (3)–(9) and steps (11)–(19) that would reconcile the heat of CH_4 adsorption, yet retain the rate expression, is to alter steps (4) and (5) to

$$\mathrm{CH_4 + S \overset{K_{CH_4}}{\not\leftarrow\!\!\!\rightarrow} CH_3^{\ominus}\text{–}S\text{–}H^{\oplus}}, \tag{4a}$$

$$\mathrm{NO\text{–}S + CH_3^{\ominus}\text{–}S\text{–}H^{\oplus} \xrightarrow{k} HNO\text{–}S\text{–}H + CH_3\text{–}S} \quad \text{(rds)}; \tag{5a}$$

and steps (12) and (15) to

$$2\left[\mathrm{CH_4 + S \overset{K_{CH_4}}{\not\leftarrow\!\!\!\rightarrow} CH_3^{\ominus}\text{–}S\text{–}H^{\oplus}}\right], \tag{12a}$$

Table 5
Comparison of NO_x reduction catalysts in the presence of O_2 and H_2O

Catalyst	Temp	Reductant		H_2O	NO	O_2	Bal	N_2 Rate	N_2 Activity	TOF	GHSV	α[a]	Reference
	(K)		%	%	%	%		μmol/s g×10^3	μmol/s m^2 × 10^3	s^{-1} × 10^3	h^{-1}	%	
La_2O_3/Al_2O_3	923	CH_4	0.35	2.0	1.4	1.0	He	770	8.1	17	100,000	33	This study
Y_2O_3	923	CH_4	0.40	2.0	0.40	0.40	He	60	0.50	n/a[e]	30,000	12	[18]
Co/Al_2O_3	923	C_3H_6	0.06	20	0.07	3.0	N_2	75	0.46	n/a[e]	21,000	n/a[f]	[19]
La_2O_3/Al_2O_3	873	CH_4	0.35	2.0	1.4	1.0	He	420	4.4	9.1	100,000	39	This study
Co/ZSM-5	873	CH_4	0.10	0[c]	0.10	2.0	He	67[d]	n/a[b]	n/a[e]	40,000	14	[20]
Co–La/ZSM-5	873	CH_4	0.10	0[c]	0.10	2.0	He	104[d]	n/a[b]	n/a[e]	40,000	21	[20]
Ce–Ag/ZSM-5	873	CH_4	0.50	8.3	0.50	2.5	He	60[d]	n/a[b]	2.4	7,500	31	[21]
In/ZSM-5	873	CH_4	0.10	10	0.10	10	He	15[d]	n/a[b]	n/a[e]	30,000	n/a[f]	[22]
Co/ZSM-5	873	CH_4	0.10	2.0	0.09	2.5	He	70[d]	n/a[b]	0.21	30,000	9	[23]
Co/Ferrierite	873	CH_4	0.10	2.0	0.09	2.5	He	101[d]	n/a[b]	0.30	30,000	14	[23]
Co/Al_2O_3	873	C_3H_6	0.06	20	0.07	3.0	N_2	98	0.60	n/a[e]	21,000	n/a[f]	[19]
$Sn–Co/Al_2O_3$	873	C_3H_6	0.06	20	0.07	3.0	N_2	84	0.51	n/a[e]	21,000	n/a[f]	[19]
La_2O_3/Al_2O_3	823	CH_4	0.35	2.0	1.4	1.0	He	142	1.5	3.1	100,000	39	This study
Co/Ferrierite	823	CH_4	0.10	2.0	0.40	2.5	He	60	n/a[b]	2.7	30,000	17	[24]
Cu/Al_2O_3	823	C_3H_6	0.20	5.0	0.2	5.0	He	56	n/a[b]	0.30	15,000[d]	14	[25]
Co/Al_2O_3	823	C_3H_6	0.06	20	0.07	3.0	N_2	75	0.46	n/a[e]	21,000	n/a[f]	[19]
$Sn–Co/Al_2O_3$	823	C_3H_6	0.06	20	0.07	3.0	N_2	88	0.54	n/a[e]	21,000	n/a[f]	[19]
Ag/Al_2O_3	823	C_3H_6	0.10	3.0	0.10	5.0	N_2	250	1.3	n/a[e]	40,000	25	[26]
La_2O_3/Al_2O_3	773	CH_4	0.35	2.0	1.4	1.0	He	37	0.39	0.81	100,000	37	This study
Fe/ZSM-5	773	C_4H_{10}	0.50	10	0.20	3.0	He	290	n/a[b]	0.60	42,000	14	[27]
Fe/ZSM-5	773	C_4H_{10}	0.20	20	0.20	3.0	He	990	n/a[b]	2.5	42,000	> 9	[28]
Co/Al_2O_3	773	C_3H_6	0.06	20	0.07	3.0	N_2	19	0.12	n/a[e]	21,000	n/a[f]	[19]
$Sn–Co/Al_2O_3$	773	C_3H_6	0.06	20	0.07	3.0	N_2	75	0.46	n/a[e]	21,000	n/a[f]	[19]

[a] Defined in Eq. (1).
[b] Specific surface area not reported.
[c] Steamed for 24 h in 114 Torr of H_2O at 1073 K.
[d] Assumed catalyst density of 1 g/cm^3.
[e] Neither NO uptake nor reactive sites reported.
[f] CH_4 conversion data not reported.

$$2\left[NO_2–S + CH_3^{\ominus}–S–H^{\oplus} \xrightarrow{k} HNO_2–S + CH_3–S\right] \quad \text{(rds)}, \tag{15a}$$

where S represents an oxygen vacancy with its neighboring atoms.

Finally, with satisfactory rate expressions for NO reduction in the presence of O_2 and CO_2 over both La_2O_3 [7] and γ-Al_2O_3, one should be able to fit the rate data in Fig. 12 using the rate constants from the two independent optimization routines if the appropriate contribution from each surface is known. Since the rates are presented on an areal basis, the two rate expressions must be multiplied by weighting factors corresponding to the fractional surface area of each oxide such that the overall rate for CH_4 disappearance over 40% La_2O_3/γ-Al_2O_3 is represented by

$$r_{La_2O_3/Al_2O_3} = X r_{La_2O_3} + (1 - X) r_{Al_2O_3}, \tag{24}$$

where $r_{La_2O_3}$ is defined by Eq. (21), $r_{Al_2O_3}$ is defined by Eq. (23), and X is the area fraction of La_2O_3 in the catalyst. Using Eq. (24), X was optimized to fit the data, as shown in Fig. 12, this yielded a value of 0.068 for the area fraction of La_2O_3. This estimate of the La_2O_3 area fraction indicates that even though a 40 wt% loading of La_2O_3 represents $1\frac{1}{2}$ theoretical monolayers, there is considerable agglomeration, which exposes a large portion of the γ-Al_2O_3. This is consistent with XRD results because line-broadening analyses were conducted on the XRD patterns using the Scherrer equation to calculate the crystallite size of La_2O_3 and Al_2O_3 in the supported sample [14,42]. The average crystallite size for γ-Al_2O_3 was 9.2 nm, which translates into 168 m^2/g and is consistent with the BET surface area of 150 m^2/g, while the average crystallite size for La_2O_3 was 56 nm, which indicates a surface area of 16.4 m^2/g. Based on these two values and a 40 wt% La_2O_3 loading, the estimated fraction of surface area comprosed of La_2O_3 is 0.061, which is in good agreement with the X value from optimization.

5. Summary

The reversible inhibitory effect on the rate of NO reduction by CH_4 over 40% La_2O_3/γ-Al_2O_3 due to either CO_2 or H_2O is similar to that observed with unsupported La_2O_3; however, the extent of rate inhibition is considerably smaller compared to the unsupported catalyst. With no O_2 in the feed, a previous reaction model for La_2O_3 was able to describe the kinetic behavior very well for all components after competitive CO_2 and H_2O adsorption was incorporated

Table 6
Optimized rate parameters from the data-fitting routine for Eq. (10) in the absence of O_2 (either CO_2 or H_2O) and Eqs. (20) and (23) in the presence of O_2

	k'_{NO} [a]	k'_{com} [b]	K_{NO} ($Torr^{-1}$)	K_{CH_4} ($Torr^{-1}$)	K_{O_2} ($Torr^{-1}$)	K_{CO_2} ($Torr^{-1}$)	K_{H_2O} ($Torr^{-1}$)
			CO_2 study				
O_2 absent							
973 K	0.00074	–	0.15	0.91	–	0.0030	–
948 K	0.0010	–	0.25	1.0	–	0.0074	–
923 K	0.0018	–	0.36	1.9	–	0.013	–
O_2 present							
La_2O_3 [from Ref. [7]]							
923 K	0.014	0.21	0.042	0.55	0.37	0.0042	–
898 K	0.023	0.46	0.15	0.60	0.59	0.010	–
873 K	0.025	0.054	0.16	0.91	0.65	0.017	–
γ-Al_2O_3			[K'_{NO_2} [c]]				
923 K	0.00041	0.0034	*0.057*	0.76	–	–	–
898 K	0.00064	0.0032	*0.059*	1.1	–	–	–
873 K	0.0011	0.0049	*0.085*	1.6	–	–	–
848 K	0.0033	0.012	*0.18*	3.8	–	–	–
			H_2O study				
O_2 absent							
973 K	0.0087	–	–	1.1	–	–	0.058
948 K	0.0003	–	–	0.72	–	–	0.031
923 K	0.0011	–	–	1.9	–	–	0.086
898 K	0.0012	–	–	2.5	–	–	0.15
O_2 present							
873 K	0.042	0.85	0.55	0.88	15	–	0.26
848 K	0.086	2.3	1.1	0.65	92	–	0.35
823 K	0.13	1.4	1.9	1.5	140	–	1.1
798 K	0.090	2.4	2.6	3.7	180	–	0.91

[a] Units for k'_{NO} are μmol N_2 $(s\,m^2\,Torr^2)^{-1}$ in the absence of O_2 and μmol N_2 $(s\,m^2\,Torr^{2.5})^{-1}$ in the presence of O_2.
[b] Units for k'_{com} are μmol CH_4 $(s\,m^2\,Torr^{1.5})^{-1}$.
[c] Units for K'_{NO_2} (defined in Eq. (22)) are $Torr^{-1.5}$ and apply only to γ-Al_2O_3.

Table 7
Enthalpies and entropies of adsorption based on the equilibrium adsorption constants from Table 6 and a previous study in the absence of O_2 with no CO_2 or H_2O in the feed[a]

	NO[b]	CH_4[b]	O_2[b]	CO_2[b]	H_2O[b]
		Huang et al. [4]			
O_2 absent					
ΔH°_{ad}	−28	−20	–	–	–
ΔS°_{ad}	−23	−9	–	–	–
		CO_2 study			
O_2 absent					
ΔH°_{ad}	−31 ± 3	−25 ± 10	–	−52 ± 8	–
ΔS°_{ad}	−22 ± 3	−13 ± 9	–	−52 ± 8	–
O_2 present					
La_2O_3 [7]					
ΔH°_{ad}	−43 ± 20	−21 ± 7	−35 ± 15	−44 ± 7	–
ΔS°_{ad}	−40 ± 20	−11 ± 7	−28 ± 15	−45 ± 7	–
γ-Al_2O_3					
ΔH°_{ad}	−32 ± 4	–	–	–	
ΔS°_{ad}	–	−23 ± 5	–	–	–
		H_2O study			
O_2 absent					
ΔH°_{ad}	–	−24 ± 13	–	–	−28 ± 18
ΔS°_{ad}	–	−12 ± 12	–	–	−22 ± 16
O_2 present					
ΔH°_{ad}	−28 ± 4	−29 ± 11	−45 ± 17	–	−27 ± 10
ΔS°_{ad}	−20 ± 4	−21 ± 13	−32 ± 20	–	−20 ± 12

[a] Values of ΔH°_{ad} are in kcal/mol, values of ΔS°_{ad}—cal/mol K.
[b] Confidence limits of 90%.

into the model to give the following rate expression:

$$r_{N_2} = k' P_{NO} P_{CH_4} \times \left(1 + K_{NO} P_{NO} + K_{CH_4} P_{CH_4} + K_{CO_2} P_{CO_2} + K_{H_2O} P_{H_2O}\right)^{-2}.$$

This equation fit the data well and gave thermodynamically consistent parameters.

With excess O_2 in the feed, when H_2O was also added, a rate equation proposed earlier for La_2O_3 was capable of providing a good fit of the data with thermodynamically consistent parameters under integral reaction operation. However, with both CO_2 and excess O_2 in the feed, this rate expression for La_2O_3 could not provide thermodynamically meaningful parameters from the fitting constants. This was attributed to a major contribution from the alumina because CO_2 had no significant effect on the reaction over alumina, but it inhibited that on La_2O_3. For Al_2O_3, the reaction model was altered by assuming that NO_2, rather than NO, was the principal N-containing intermediate on the alumina surface. This led to the rate expression for total CH_4 disappearance due to both NO reduction and combustion on γ-Al_2O_3

$$(r_{CH_4})_T = \left(k'_{com} P_{CH_4} P_{O_2}^{0.5} + k'_{NO} P_{NO} P_{CH_4} P_{O_2}^{0.5}\right) \times \left(1 + K'_{NO_2} P_{NO} P_{O_2}^{0.5} + K_{CH_4} P_{CH_4} + K_{O_2}^{0.5} P_{O_2}^{0.5} + K_{CO_2} P_{CO_2} + K_{H_2O} P_{H_2O}\right)^{-2},$$

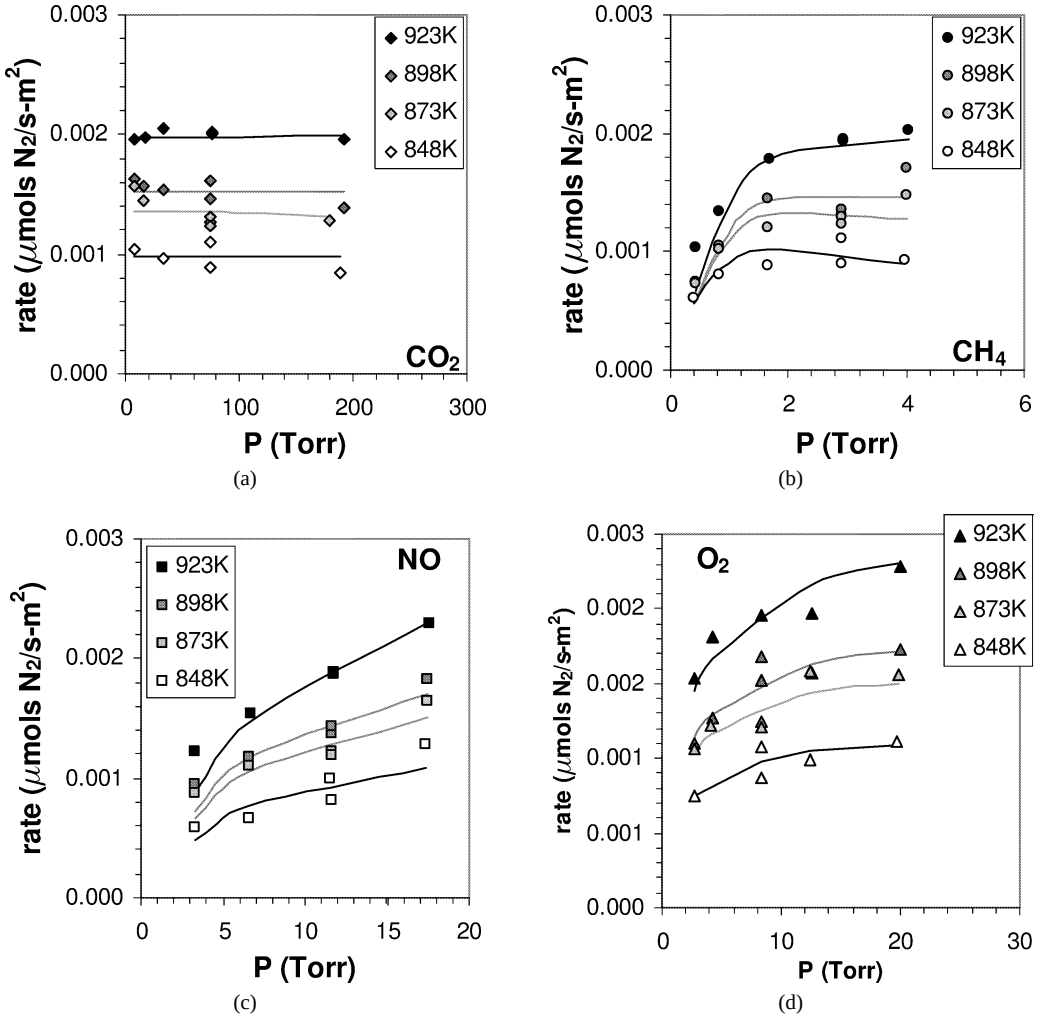

Fig. 15. Partial pressure dependencies in excess CO_2 for NO reduction by CH_4 over γ-Al_2O_3 with O_2 in the feed for (a) CO_2, (b) CH_4, (c) NO, and (d) O_2. Experimental data are represented by symbols and the expression given by Eq. (23) is represented by lines. Reaction conditions: 1.4% NO, 0.35% CH_4, 1.0% O_2, and 9% CO_2, balance He; GHSV = 85,000 h^{-1}.

which gave satisfactory fits to the data and thermodynamically consistent parameters, assuming that dissociative CH_4 adsorption occurred on a site which presumably consists of an oxygen vacancy and its neighboring atoms. This equation was then combined with the rate equation describing NO reduction on pure La_2O_3 in the presence of O_2, and the data were fit well, assuming that La_2O_3 occupied 6.8% of the total surface area, a value in good agreement with that of 6.1% obtained from XRD line-broadening calculations.

Table 8
Reaction orders for NO reduction by CH_4 over γ-Al_2O_3 in the presence of O_2 with CO_2 in the feed

	NO	CH_4	O_2	CO_2	H_2O
		CO_2 study			
O_2 present					
923 K	0.33	0.30	0.17	0.00	–
908 K	0.30	0.29	0.23	−0.04	–
893 K	0.27	0.27	0.19	−0.08	–
873 K	0.35	0.20	0.19	−0.05	–

Reaction conditions: 1.4% NO, 0.35% CH_4, 1.0% O_2, 9.0% CO_2, balance He; GHSV = 85,000 h^{-1}.

Acknowledgment

This study was supported by the National Science Foundation under Grant CTS-9633752.

References

[1] X. Zhang, A.B. Walters, M.A. Vannice, Appl. Catal. B 4 (1994) 237.
[2] X. Zhang, A.B. Walters, M.A. Vannice, J. Catal. 155 (1995) 290.
[3] X. Zhang, A.B. Walters, M.A. Vannice, Catal. Today 27 (1996) 41.
[4] S.-J. Huang, A.B. Walters, M.A. Vannice, Appl. Catal. B 17 (1998) 183.
[5] C. Shi, A.B. Walters, M.A. Vannice, Appl. Catal. B 14 (1997) 175.
[6] S.-J. Huang, A.B. Walters, M.A. Vannice, Appl. Catal. B 26 (2000) 101.

[7] T.J. Toops, A.B. Walters, M.A. Vannice, Appl. Catal. B 38 (2002) 183.
[8] R.B. Bagwell, G.L. Messing, J. Am. Ceram. Soc. 82 (1999) 825.
[9] M. Pijolat, M. Dauzat, M. Soustelle, Solid State Ionics 50 (1992) 31.
[10] J.M. McHale, A. Navrotsky, J. Phys. Chem. B 101 (1997) 603.
[11] W.-P. Tai, T. Watanabe, J. Am. Ceram. Soc. 82 (1999) 245.
[12] T.J. Toops, A.B. Walters, M.A. Vannice, Catal. Lett. 82 (2002) 45.
[13] T.J. Toops, A.B. Walters, M.A. Vannice, Appl. Catal. A 233 (2002) 125.
[14] T.J. Toops, PhD thesis, Pennsylvania State University, 2001.
[15] T.J. Toops, A.B. Walters, M.A. Vannice, Catal. Lett. 64 (2000) 65.
[16] B. Klingenberg, M.A. Vannice, Chem. Mater. 8 (1996) 2755.
[17] M.P. Rosynek, D.T. Magnuson, J. Catal. 46 (1977) 402.
[18] M.D. Fokema, J.Y. Ying, Appl. Catal. B. 18 (1998) 71.
[19] L. Chen, T. Horiuchi, T. Mori, Catal. Lett. 72 (2001) 71.
[20] P. Budi, R. Howe, Catal. Today 38 (1997) 175.
[21] Z. Li, M. Flytzani-Stephanopolous, Appl. Catal. B 22 (1999) 35.
[22] E. Kikuchi, M. Ogura, N. Aratani, Y. Sugiura, S. Hiromoto, K. Yogo, in: G. Centi, S. Perathoner, C. Christani, P. Forzatti (Eds.), Environmental Catalysis, Rome, Italy, 1995, p. 27.
[23] Y. Li, J.N. Armor, Appl. Catal. B 5 (1995) L257.
[24] Y. Li, J.N. Armor, J. Catal. 150 (1994) 376.
[25] E.A. Efthimidias, G.D. Lionta, S.C. Christoforou, I.A. Vasalos, Catal. Today 40 (1998) 15.
[26] A. Martinez-Arias, M. Fernandez-Garcia, A. Iglesias-Juez, J.A. Anderson, J.C. Conesa, J. Soria, Appl. Catal. B 28 (2000) 29.
[27] H.-Y. Chen, W.M.H. Sachtler, Catal. Today 42 (1998) 73.
[28] X. Feng, W.K. Hall, J. Catal. 166 (1997) 368.
[29] M. Pijolat, M. Dauzat, M. Soustelle, Solid State Ionics 50 (1992) 31.
[30] H. Schaper, D.J. Amesz, E.B.M. Doesburg, L.L. Van Reijen, Appl. Catal. 9 (1984) 129.
[31] M. Bettman, R.E. Chase, K. Otto, W.H. Weber, J. Catal. 117 (1989) 447.
[32] H. Schaper, E.B.M. Doesburg, L.L. Van Reijen, Appl. Catal. 7 (1983) 211.
[33] B. Klingenberg, M.A. Vannice, Appl. Catal. B 21 (1999) 19.
[34] H. Wijnja, C.P. Schulthess, Spectrochim. Acta Part A 55 (1999) 861.
[35] M.A. Vannice, A.B. Walters, X. Zhang, J. Catal. 159 (1996) 119.
[36] M. Boudart, AIChE J. 18 (1972) 465.
[37] M.A. Vannice, S.H. Hyun, B. Kalpakci, W.C. Liauh, J. Catal. 56 (1979) 358.
[38] W.S. Klijstra, D.S. Brands, E.K. Poels, A. Bliek, J. Catal. 171 (1997) 208.
[39] M.J. Capitan, J.A. Odriozola, A. Marquez, J.F. Sanz, J. Catal. 156 (1995) 273.
[40] T. Ito, T. Tashiro, T. Kawasaki, M. Watanabe, K. Toi, H. Kobayashi, J. Phys. Chem. 95 (1991) 4476.
[41] S.-J. Huang, A.B. Walters, M.A. Vannice, J. Catal. 192 (2000) 29.
[42] B.D. Cullity, Elements of X-Ray Diffraction, Addison–Wesley, Reading, MA, 1956.